

Article

The Carbon-Coated ZnCo_2O_4 Nanowire Arrays Pyrolyzed from PVA for Enhancing Lithium Storage Capacity

Wenjia Zhao ^{1,*}, Zhaoping Shi ¹, Yongbing Qi ¹ and Jipeng Cheng ^{2,3,*} 

¹ Department of Chemistry, College of Sciences, Nanjing Agricultural University, Nanjing 210095, China; 23217220@njau.edu.cn (Z.S.); 23217208@njau.edu.cn (Y.Q.)

² School of Materials Science and Engineering, Zhejiang University, Hangzhou 310027, China

³ School of Physics and Microelectronics, Zhengzhou University, Zhengzhou 450052, China

* Correspondence: zhaowenjia@njau.edu.cn (W.Z.); chengjp@zju.edu.cn (J.C.)

Received: 20 October 2020; Accepted: 17 November 2020; Published: 20 November 2020



Abstract: In this paper, ZnCo_2O_4 nanowire arrays with a uniform carbon coating were introduced when polyvinyl alcohol (PVA) served as the carbon source. The coating process was completed by a facile bath method in PVA aqueous solution and subsequent pyrolyzation. The PVA-derived carbon-coated ZnCo_2O_4 nanowire array composites can be used directly as the binder-free and self-supported anode materials for lithium-ion batteries. In the carbon-coated ZnCo_2O_4 composites, the carbon layer carbonized from PVA can accelerate the electron transfer and accommodate the volume swing during the cycling process. The lithium storage properties of the carbon-coated ZnCo_2O_4 composites are investigated. It is believed that the novel carbon-coating method is universal and can be applied to other nanoarray materials.

Keywords: polyvinyl alcohol; carbon coating; nanoarray composites; lithium-ion batteries

1. Introduction

Nowadays, a variety of electric vehicles and portable electronic devices (mobile phones, laptops, etc.) have been widely applied and developed rapidly in the world. Lithium-ion batteries as requisite energy storage devices for them receive more demand than ever before [1–4]. The commercial graphite anode has low theoretical capacity of $372 \text{ mA}\cdot\text{h}\cdot\text{g}^{-1}$ and awkward rate performance. Hence, it is imperative to study and find promising alternate materials. In recent studies, transition metal oxides (TMOs) have attracted growing interest owing to their large theoretical capacities ($>600 \text{ mA}\cdot\text{h}\cdot\text{g}^{-1}$) [5–8]. ZnCo_2O_4 , as one of the cobalt-based materials, stands out among a variety of anode materials for its high reversible capacities ($976 \text{ mA}\cdot\text{h}\cdot\text{g}^{-1}$) and environmental benignity [9–14]. Nevertheless, poor electric conductivity and cycling stability still need improvement to realize its commercialization [15,16].

Recent research indicates that the free-standing nanoarray construction of electrode materials can effectively shorten the transport path of electrons and ions, alleviate the volume swings caused by the repeated ion insertion/extraction, as well as avoid the use of additional binder and conductive agent. These nanoarray electrodes displayed outstanding cycling stability and rate performance [17–23]. Wang et al. reported the fabrication of NiCo_2O_4 nanowire arrays grown on carbon cloth as a binder-free electrode for both sodium and lithium-ion storage. Subsequently, an amorphous carbon layer has been deposited onto the surface of the NiCo_2O_4 nanowires through the physical vapor deposition technique, further improving the conductivity and structural stability of the materials [24]. Wang and his co-workers at Tianjin University reported free-standing electrode of Fe_2O_3 nanorods grown on the carbon fiber. They then coated Fe_2O_3 with carbon by a hydrothermal method in an aqueous solution

containing glucose heated at 200 °C for 4 h [25]. Hence, the carbon coating can significantly enhance the electrochemical performances of active materials. However, the existing methods of coating on the nanoarrays are always complicated, either rely on the expensive instrument (e.g., CVD, PECVD, or ALD), or require high reaction temperature [26–30].

In this paper, we present a novel and facile in situ bath method in polyvinyl alcohol (PVA) aqueous solution to fabricate carbon-coated ZnCo₂O₄ nanoarrays. The composites not only benefit the advantages of nanoarray architecture but also the introduction of a uniform carbon layer can greatly strengthen the electroconductivity and structural stability, leading to better electrochemical performance. Our work of the novel carbon-coating method has versatility and can be used to optimize the electrochemical performance of other electrode materials.

2. Experimental

2.1. Synthesis of Carbon-Coated ZnCo₂O₄ Nanowire Arrays

The ZnCo₂O₄ nanowire arrays directly grown on the Ni foam were obtained according to the literature reported by our group [31]. Firstly, a mixed solution of 2 mM Zn(NO₃)₂·6H₂O, 4 mM Co(NO₃)₂·6H₂O, 4 mM NH₄F, and 10 mM CO(NH₂)₂ was transferred into a Teflon-lined stainless steel autoclave. Then, a piece of Ni foam was placed into the solution with its top side covered by a PTFE (Poly tetra fluoroethylene) tape. The autoclave was maintained at 120 °C for 6 h and then annealed at 400 °C for 2 h in air. Subsequently, 0.3% wt. concentrations of PVA (PVA-105, Aladdin, Shanghai, China) solutions were prepared and kept ultrasonication for about half an hour to remove the bubbles. The as-prepared ZnCo₂O₄ nanowire arrays were immersed into the PVA solutions for about 10 min and then freeze-dried for 24 h. Finally, the carbon-coated arrays were obtained by heat treatment at 500 °C for 2 h in an argon flow.

2.2. Materials Characterization

The X-ray diffraction (XRD) measurements were operated on a Rigaku D/max 2550 PC diffractometer using Cu K α radiation ($\lambda = 1.5418 \text{ \AA}$). The morphology and microstructure of samples were characterized by scanning electron microscopy (SEM, Hitachi, Tokyo, Japan, SU8010) and transmission electron microscopy (TEM, FEI, Hillsboro, OR, USA, F20). Thermogravimetric analysis (TGA) was performed in air with a temperature range of 25 °C to 800 °C to measure the carbon content in samples. Raman spectroscopic measurement was done using a NTEGRA Spectra AFM Raman Confocal SNOM instrument.

2.3. Electrochemical Measurement

The electrochemical tests were conducted using 2032 coin-type cells. These cells were assembled in an Ar-filled glove box ($O_2 \leq 0.1 \text{ ppm}$, $H_2O \leq 0.1 \text{ ppm}$), with the prepared samples directly as working electrode, lithium foil as counter/reference electrode. The electrolyte was a 1 M solution of LiPF₆ in ethylene carbonate (EC) and Dimethyl carbonate (DMC) (1:1 by volume). Galvanostatic charge-discharge tests of cells were taken on a LAND test system in the voltage range of 0.01 and 2.5 V (vs. Li/Li⁺) at room temperature.

3. Results and Discussion

The XRD patterns of the ZnCo₂O₄ and carbon-coated ZnCo₂O₄ samples have been shown in Figure 1a and Figure 1b, respectively. Before the XRD test, in order to separate the nanomaterials from the nickel foam, the samples were wildly ultrasonicated for 30 min. It can be seen that both of the samples display well-defined peaks at 31.2, 36.8, 38.5, 44.7, 55.6, 59.3, and 65.1°, which can be indexed to the (220), (311), (222), (400), (422), (511) and (440) planes of spinel ZnCo₂O₄ (PDF No. 23–1390). Moreover, no obvious peaks related to the carbon have been found in the XRD patterns in Figure 1b, which can be ascribed to the amorphous nature of the carbon layer.

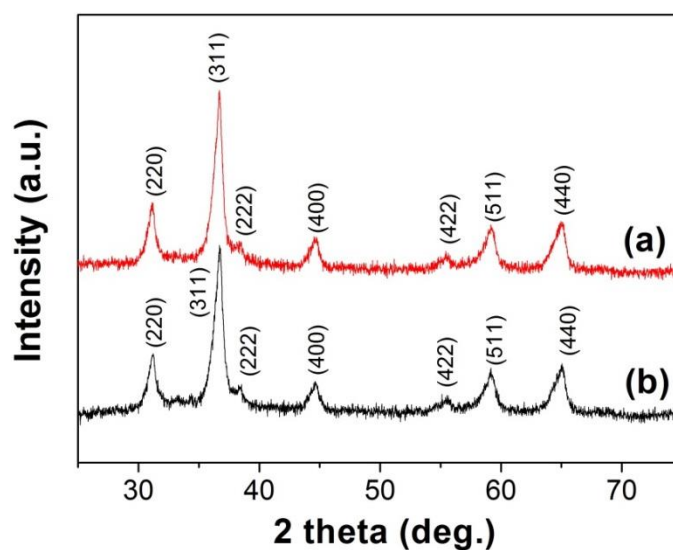


Figure 1. XRD patterns of (a) ZnCo_2O_4 and (b) carbon-coated ZnCo_2O_4 samples.

Figure 2 exhibits the characterizations of the morphology, structure, and composition of the carbon-coated ZnCo_2O_4 nanostructures. Figure 2a shows the SEM image of the carbon-coated ZnCo_2O_4 nanowires directly grown on the nickel foam. The nanocomposites still maintain the nanowire array structure after the immersion and thermal treatment process compared with the original ZnCo_2O_4 . The specific characterizations of the morphology of bare ZnCo_2O_4 nanowire arrays can be referred to in our pre-published literature [31]. Figure 2b displays the TEM image of the carbon-coated ZnCo_2O_4 nanowires, in which more structural details can be seen. The ZnCo_2O_4 nanowires are polycrystalline and consist of numerous nanoparticles. However, in neither SEM nor TEM images, can the carbon coating layer be obviously observed. Figure 2d gives a partial enlarged TEM image of a single carbon-coated ZnCo_2O_4 nanowire. In Figure 2d, one can clearly see that the nanowire has been completely and uniformly surrounded by an amorphous layer. In comparison to the carbon-coated samples, a TEM image of the bare ZnCo_2O_4 nanowire was illustrated in Figure 2c. Without the amorphous layer, the polycrystalline nanoparticles look more distinct. The compositional line profiles of the uncoated and coated nanowires are revealed in Figure 2e,f. In Figure 2f, there are significant signals of the Energy Dispersive X-Ray Spectroscopy (EDX) for Zn, Co, O, and C elements, which are expected to stem from ZnCo_2O_4 and carbon layer, respectively. The corresponding line-scan EDX patterns further confirm the presence and location of the carbon layer. The HRTEM (Figure 2g) of the carbon-coated ZnCo_2O_4 further indicates that the thickness of the coating layer is about 3 nm. The completeness, continuity, and suitable thickness of a carbon coating layer on the surface of the electrode materials is of great importance for the electrochemical reactions. If the coating layer is too thick, it may lead to negative effects for the ions to pass through; while too thin coating layers may not effectively maintain the micro-structure of the active materials. It has been reported that the thickness of about 2–3 nm of the carbon coating layer may be appropriate for repetitive insertion/extraction of ions [32–34]. In Figure 2g, there are distinct lattice fringes with lattice spacings of about 0.233 and 0.286 nm, corresponding to (222) and (220) planes of ZnCo_2O_4 , respectively. The selected area electron diffraction (SAED) pattern of the carbon-coated ZnCo_2O_4 in Figure 2h is comprised of sets of concentric rings with occasional bright spots which indicate the nano-crystalline nature of the composites. The diffraction rings can be readily assigned to the crystal planes of the spinel ZnCo_2O_4 phase. These outcomes suggest that the carbon-coated ZnCo_2O_4 core-shell nanostructures have been successfully manufactured after the immersion in PVA solution and subsequent carbonization process.

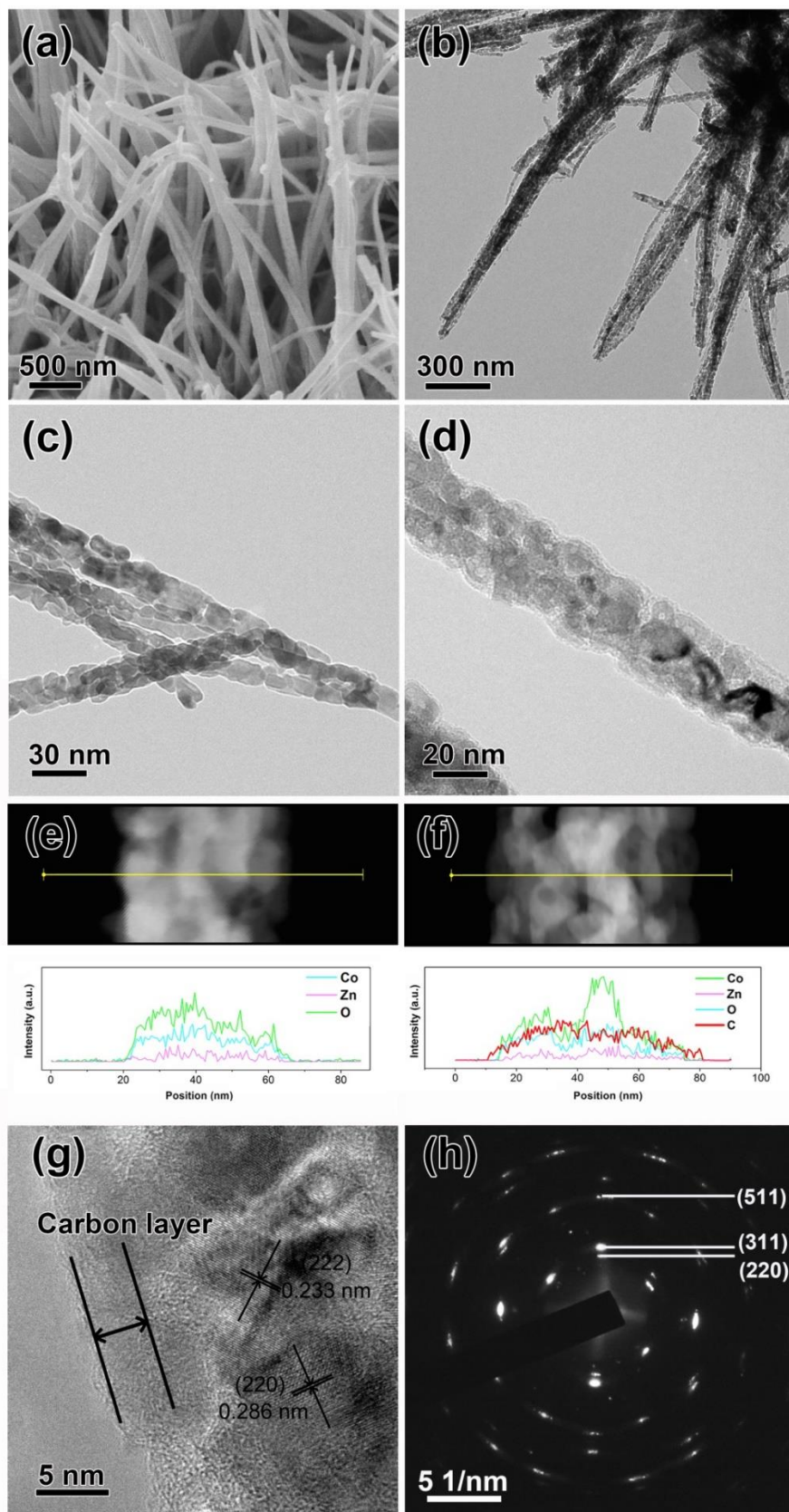


Figure 2. (a) A SEM image, (b) a TEM image of carbon-coated ZnCo_2O_4 nanowires, (c,d) partially enlarged TEM images of uncoated and carbon-coated ZnCo_2O_4 nanowires, compositional line profiles across (e) the uncoated and (f) carbon-coated ZnCo_2O_4 nanowires probed by EDX spectroscopy, (g) HRTEM image, (h) SAED patterns of the carbon-coated ZnCo_2O_4 nanowires.

The presence of carbon in the composites can be further affirmed by the Raman spectrum (Figure 3a) and TGA analysis (Figure 3b). In Figure 3a, there are two distinct characteristic peaks for the carbon-coated samples. The peaks located at $\sim 1340\text{ cm}^{-1}$ are D band, representing the disordered structures or structural defects in carbon materials; while the peaks at $\sim 1590\text{ cm}^{-1}$ are G band, attributed to the degree of graphitization. Meanwhile, due to the relatively low signal intensity, the typical Raman spectrum of the uncoated samples is almost a straight line. The results of the Raman spectrum confirm the presence of carbon and partial graphitization of the carbon-coated ZnCo_2O_4 samples. TGA was carried out to measure the carbon content in the composites in the air atmosphere to $800\text{ }^\circ\text{C}$. In Figure 3b, the weight loss from 200 to $600\text{ }^\circ\text{C}$ is due to the combustion reaction of the carbon component in the composites. The carbon content of the carbon-coated ZnCo_2O_4 composites is about 16.4% by weight. The above characterizations confirm the successful synthesis of ZnCo_2O_4 -C core-shell nanocomposites.

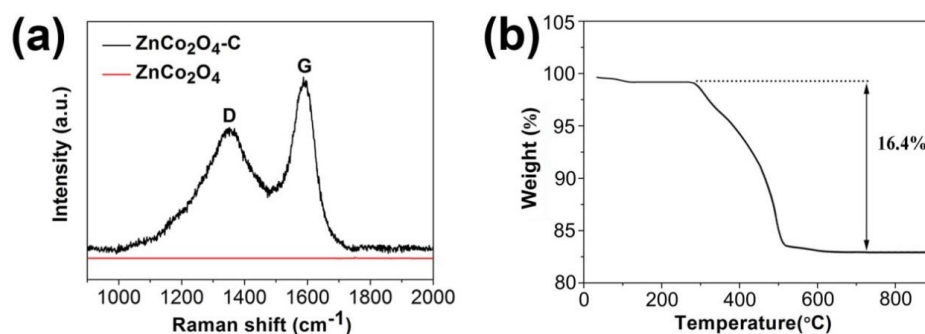


Figure 3. (a) Typical Raman spectrum of the uncoated and carbon-coated ZnCo_2O_4 , (b) TGA analysis of the carbon-coated ZnCo_2O_4 nanocomposites.

The one-dimensional nanowire structure, the orderly aligned arrays, and the uniform carbon coating make the composite a preeminent anode material for LIBs. Herein, the carbon-coated ZnCo_2O_4 nanowire arrays grown on the Ni foam are directly evaluated as the anode. Figure 4 reveals the first three cyclic voltammogram (CV) curves of the carbon-coated ZnCo_2O_4 nanowire electrodes in the potential range of 0.01 – 3.0 V at a scan rate of $0.1\text{ mV}\cdot\text{s}^{-1}$. The electrochemical reactions of ZnCo_2O_4 with Li can be clarified as follows [35,36]:

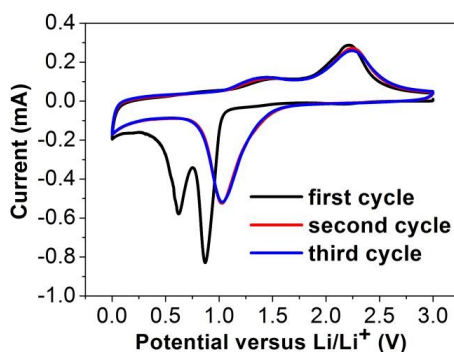
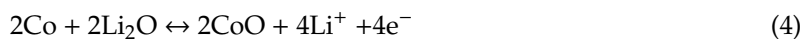
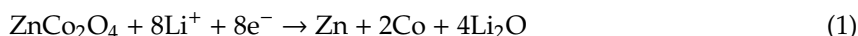


Figure 4. The first three CV curves of carbon-coated ZnCo_2O_4 array electrodes between 0.0 V to 3.0 V versus Li/Li^+ at a scan rate of $0.1\text{ mV}\cdot\text{s}^{-1}$.

It can be clearly seen that the curve of the first cathodic scan is different from the subsequent ones. In the first circle, the two reduction peaks located at 0.87 V and 0.62 V are corresponded to the reduction process of ZnCo_2O_4 to Zn and Co accompanying the formation of the SEI layer. During the first anodic scan, two broad peaks corresponding to the oxidation of metallic Zn and Co are detected at 1.4 V and 2.2 V. In the following cycles, the major reduction peak shifts to a higher potential of 1.03 V, suggesting that the polarization of the electrode material is decreased after the activation process in the initial circle. Similar reports of shifts to a higher potential in the subsequent circles have been reported [37,38]. The shape and position of anodic peaks keep stable in the following circles.

The investigation about the effects of the carbon coating on the electrochemical performance has been carried out. Figure 5a illustrates the cycling performance of the carbon-coated ZnCo_2O_4 in comparison with the pristine ZnCo_2O_4 electrode for LIBs under the same test conditions. As can be seen, the carbon-coated ZnCo_2O_4 electrodes display higher reversible capacities, compared with the untreated ZnCo_2O_4 . The bare ZnCo_2O_4 electrode goes through a rapid capacity fading, and remain the capacity of less than $300 \text{ mA}\cdot\text{h}\cdot\text{g}^{-1}$ after 100 loops. On the other hand, the reversible capacities of the carbon-coated ZnCo_2O_4 electrodes after 100 cycles were $886.4 \text{ mA}\cdot\text{h}\cdot\text{g}^{-1}$. The right amount of the carbon coating plays a significant role in the electrochemical performance of the anode materials [29–31]. If the coating layer is excessively thin, it probably cannot afford to hold the integrity of the materials during repeated ion insertion/extraction. However, coating that is too thick may block the traversing of the Li^+ ions. The uniform and moderate carbon coating is able to hold back the aggregation and pulverization of the ZnCo_2O_4 electrode, as well as accelerates the ion/electron transfer, which may be responsible for the enhanced cycling performance [39,40]. In addition, it is meaningful to make a comparison between our materials with those in the previously published literature, as illustrated in Table 1.

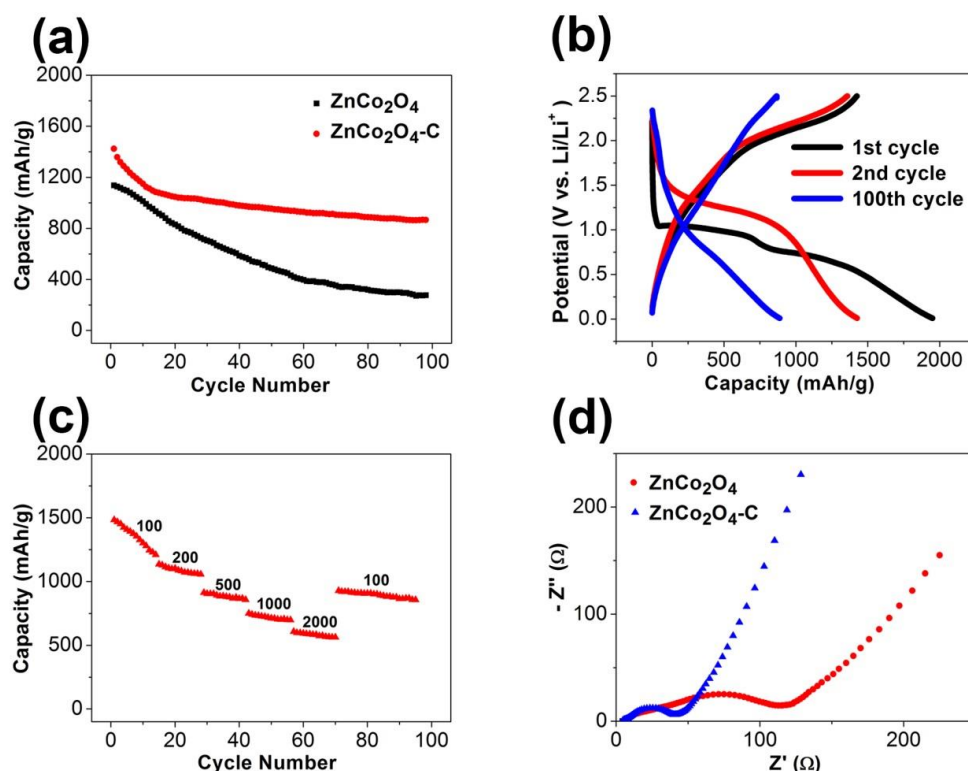


Figure 5. (a) The comparison of cycling performance of carbon-coated ZnCo_2O_4 pyrolyzed from PVA solutions with pristine ZnCo_2O_4 electrodes; (b) charge-discharge curves for lithium-ion batteries; (c) rate performance of the carbon-coated ZnCo_2O_4 pyrolyzed from PVA solution; (d) Nyquist plots of the carbon-coated and pristine ZnCo_2O_4 electrodes from 100 kHz to 0.01 Hz.

Table 1. Electrochemical performance of our carbon-coated ZnCo₂O₄ compared with those previously published Co-based anodes for LIBs.

Electrode Materials	Initial Discharge/ Charge Capacity (mA·h·g ⁻¹)	Capacity after Cycling (mA·h·g ⁻¹)	Reference
porous ZnCo ₂ O ₄	1332/979	721, 80th@100 mA g ⁻¹	[10]
ZnCo ₂ O ₄ /Co ₃ O ₄ on CC	750/736	481.9, 100th@300 mA g ⁻¹	[1]
Carbon fiber/ZnCo ₂ O ₄	927.2/613.5	787.2, 150th@100 mA g ⁻¹	[2]
CoO/hollow carbon sphere	-	584, 50th@100 mA g ⁻¹	[41]
Co@CoO	1262/956	800, 50th@50 mA g ⁻¹	[42]
CoO@C	1564/-	~800, 70th@100 mA g ⁻¹	[43]
CoO-NiO-C	1125/729	562, 60th@100 mA g ⁻¹	[44]
ZnCo ₂ O ₄ @TiO ₂	1598/1343	827, 90th@100 mA g ⁻¹	[45]
C/ZnCo ₂ O ₄ @CNT	1947.1/763.1	800.6, 100th@100 mA g ⁻¹	[46]
Co-ZnO@C	940/862	538, 50th@100 mA g ⁻¹	[47]
ZnCo ₂ O ₄ -C	1951.4/1424.5	886.4, 100th @200 mA g ⁻¹	this work

Figure 5b displays the 1st, 2nd, and 100th discharge-charge curves of the carbon-coated ZnCo₂O₄ anode material at a current density of 200 mA g⁻¹. The obvious plateau at about 1.0 V and 0.7 V were observed in the first discharge curve, which is also consistent with the CV results. The initial discharge and charge capacities reached 1951.4 mA·h·g⁻¹ and 1424.5 mA·h·g⁻¹, respectively. The capacity loss primarily dates from the formation of SEI and irreversible reactions of the electrode materials.

The carbon-coated ZnCo₂O₄ anode material also demonstrated a remarkable rate performance in Figure 5c. When the current densities reached 100, 200, 500, 1000, and 2000 mA g⁻¹, the reversible capacity reached 1210.0, 1056.4, 858.3, 698.5, and 562.8 mA·h·g⁻¹, respectively. When the current densities return to 100 mA g⁻¹, the reversible capacity can be recovered to 857.1 mA·h·g⁻¹, which is ~70.8% of the initial reversible capacity.

Electrochemical impedance spectroscopy (EIS) was processed to evaluate the charge transfer properties of the electrode materials after 5 cycles in Figure 5d. The flat semicircle in the high-frequency region is ascribed to the charge transfer resistance (R_{ct}) for the anode materials after cycling [48–50]. The Nyquist plots uncover that the diameters of the semicircles of the carbon-coated ZnCo₂O₄ electrodes are significantly smaller than that of the bare ZnCo₂O₄ electrode. From the above, the EIS results show that the coating of a layer of carbon is conducive to the reduction of the charge transfer resistance, further improving the electronic conductivity and electrochemical performance. The interface of the electrode materials for the lithium-ion batteries is one of the key issues for its long-term development, and deeper research in the future is essential [51].

4. Conclusions

In summary, we have proposed an in-situ bath method to uniformly coat ZnCo₂O₄ nanowire arrays with a carbon shell. The polymer of PVA has been chosen as the carbon source and the influence of PVA-derived carbon-coating layer on the electrochemical performance of ZnCo₂O₄ has been investigated. The carbon-coated ZnCo₂O₄ nanowire array composites can be used directly as an anode material for LIBs. The ZnCo₂O₄ nanowires directly grown on the metal substrate can enhance the electron and ion transport and avoid the additional use of binder and conductive agent. The carbon layer is able to improve the conductivity of the electrode materials and restrain the pulverization, eventually resulting in a splendid electrochemical performance.

Author Contributions: Conceptualization, W.Z. and J.C.; methodology, Z.S., Y.Q.; writing—original draft preparation, W.Z.; writing—review and editing, J.C. All authors have read and agreed to the published version of the manuscript.

Funding: This research was funded by the National Natural Science Foundation of China (51801104), the Natural Science Foundation of Jiangsu Province (BK20170726), China Postdoctoral Science Foundation (2018M632284) and Fundamental Research Fund for the Central Universities, Nanjing Agricultural University (KJQN201945).

Conflicts of Interest: The authors declare no conflict of interest.

References

1. Guo, S.; Liu, J.; Zhang, Q.; Wang, H. 3D porous ZnCo₂O₄/Co₃O₄ composite grown on carbon cloth as high-performance anode material for lithium-ion battery. *Mater. Lett.* **2020**, *267*, 127549. [[CrossRef](#)]
2. Han, Q.; Zhang, X.; Zhang, W.; Li, Y.; Zhang, Z. Preparation of multifunctional structural P-CF@ZnCo₂O₄ composites used as structural anode materials. *J. Alloy Compd.* **2020**, *842*, 155743. [[CrossRef](#)]
3. Liang, H.; Wu, J.; Wang, M.; Fan, H.; Zhang, Y. Pseudocapacitance-dominated high-performance and stable lithium-ion batteries from MOF-derived spinel ZnCo₂O₄/ZnO/C heterostructure anode. *Dalton Trans.* **2020**, *49*, 13311–13316. [[CrossRef](#)]
4. Sun, R.; Qin, Z.; Li, Z.; Fan, H.; Lu, S. Binary zinc-cobalt metal-organic framework derived mesoporous ZnCo₂O₄@NC polyhedron as a high-performance lithium-ion battery anode. *Dalton Trans.* **2020**, *49*, 14237–14242. [[CrossRef](#)]
5. Wang, L.; Li, D.; Zhang, J.; Song, C.; Xin, H.; Qin, X. Porous flower-like ZnCo₂O₄ and ZnCo₂O₄@C composite: A facile controllable synthesis and enhanced electrochemical performance. *Ionics* **2020**, *26*, 4479–4487. [[CrossRef](#)]
6. Wang, Y.; Feng, J.; Wang, H.; Zhang, M.; Yang, X.; Yuan, R.; Chai, Y. Fabricating porous ZnO/Co₃O₄ microspheres coated with N-doped carbon by a simple method as high capacity anode. *J. Electroanal. Chem.* **2020**, *873*, 114479. [[CrossRef](#)]
7. Xiao, H.; Ma, G.; Tan, J.; Ru, S.; Ai, Z.; Wang, C. Three-dimensional hierarchical ZnCo₂O₄@C₃N₄-Bnanoflowers as high-performance anode materials for lithium-ion batteries. *RSC Adv.* **2020**, *10*, 32609–32615. [[CrossRef](#)]
8. Xu, H.; Zhang, Y.; Song, X.; Kong, X.; Ma, T.; Wang, H. Synthesis of porous ZnCo₂O₄ micro-cube with large tap density and its application in anode for lithium-ion battery. *J. Alloy Compd.* **2020**, *821*, 153289. [[CrossRef](#)]
9. Cao, X.; Yang, Y.; Li, A. Facile Synthesis of Porous ZnCo₂O₄ Nanosheets and the Superior Electrochemical Properties for Sodium Ion Batteries. *Nanomaterials* **2018**, *8*, 377. [[CrossRef](#)] [[PubMed](#)]
10. Hu, L.; Qu, B.; Li, C.; Chen, Y.; Mei, L.; Lei, D.; Chen, L.; Li, Q.; Wang, T. Facile synthesis of uniform mesoporous ZnCo₂O₄ microspheres as a high-performance anode material for Li-ion batteries. *J. Mater. Chem. A* **2013**, *1*, 5596. [[CrossRef](#)]
11. Liu, W.W.; Jin, M.T.; Shi, W.M.; Deng, J.G.; Lau, W.M.; Zhang, Y.N. First-Principles Studies on the Structural Stability of Spinel ZnCo₂O₄ as an Electrode Material for Lithium-ion Batteries. *Sci. Rep.* **2016**, *6*, 36717. [[CrossRef](#)] [[PubMed](#)]
12. Xu, J.; Yan, B.; Maleki Kheimeh Sari, H.; Hao, Y.; Xiong, D.; Dou, S.; Liu, W.; Kou, H.; Li, D.; Li, X. Mesoporous ZnCo₂O₄/rGO nanocomposites enhancing sodium storage. *Nanotechnology* **2019**, *30*, 234005. [[CrossRef](#)] [[PubMed](#)]
13. Song, Y.; Zhao, M.; Pan, Z.; Jiang, L.; Jiang, Y.; Fu, B.; Xu, J.; Hu, L. Thermal transformation of ZnCo_{1.5}(OH)_{4.5}Cl_{0.5}·0.45H₂O into hexagonal ZnCo₂O₄ nanosheets for high-performance secondary ion batteries. *J. Alloy Compd.* **2019**, *783*, 455–459. [[CrossRef](#)]
14. Liu, Z.Q.; Cheng, H.; Li, N.; Ma, T.Y.; Su, Y.Z. ZnCo₂O₄ Quantum Dots Anchored on Nitrogen-Doped Carbon Nanotubes as Reversible Oxygen Reduction/Evolution Electrocatalysts. *Adv. Mater.* **2016**, *28*, 3777–3784. [[CrossRef](#)] [[PubMed](#)]
15. Gao, G.; Wu, H.B.; Dong, B.; Ding, S.; Lou, X.W. Growth of Ultrathin ZnCo₂O₄ Nanosheets on Reduced Graphene Oxide with Enhanced Lithium Storage Properties. *Adv. Sci.* **2015**, *2*, 1400014. [[CrossRef](#)]
16. Liu, B.; Zhang, J.; Wang, X.; Chen, G.; Chen, D.; Zhou, C.; Shen, G. Hierarchical three-dimensional ZnCo₂O₄ nanowire arrays/carbon cloth anodes for a novel class of high-performance flexible lithium-ion batteries. *Nano Lett.* **2012**, *12*, 3005–3011. [[CrossRef](#)]
17. Zhao, W.; Du, N.; Xiao, C.; Wu, H.; Zhang, H.; Yang, D. Large-scale synthesis of Ag-Si core-shell nanowall arrays as high-performance anode materials of Li-ion batteries. *J. Mater. Chem. A* **2014**, *2*, 13949–13954. [[CrossRef](#)]
18. Zhao, W.; Du, N.; Zhang, H.; Yang, D. A novel Co-Li₂O@Si core-shell nanowire array composite as a high-performance lithium-ion battery anode material. *Nanoscale* **2016**, *8*, 4511–4519. [[CrossRef](#)]

19. Zhao, W.; Chen, J.; Lei, Y.; Du, N.; Yang, D. A novel three-dimensional architecture of Co-Ge nanowires towards high-rate lithium and sodium storage. *J. Alloy Compd.* **2020**, *815*, 152281. [[CrossRef](#)]
20. Zhao, W.; Du, N.; Zhang, H.; Yang, D. Silver-nickel oxide core-shell nanoflower arrays as high-performance anode for lithium-ion batteries. *J. Power Sources* **2015**, *285*, 131–136. [[CrossRef](#)]
21. Zhao, W.; Du, N.; Zhang, H.; Yang, D. Silver-nickel oxide core-shell nanoparticle array electrode with enhanced lithium-storage performance. *Electrochim. Acta* **2015**, *174*, 893–899. [[CrossRef](#)]
22. Huang, R.; Fan, X.; Shen, W.; Zhu, J. Carbon-coated silicon nanowire array films for high-performance lithium-ion battery anodes. *Appl. Phys. Lett.* **2009**, *95*, 133119. [[CrossRef](#)]
23. Yang, Y.; Fu, Q.; Zhao, H.; Mi, Y.; Li, W.; Dong, Y.; Wu, M.; Lei, Y. MOF-assisted three-dimensional TiO₂@C core/shell nanobelt arrays as superior sodium ion battery anodes. *J. Alloy Compd.* **2018**, *769*, 257–263. [[CrossRef](#)]
24. Wang, K.; Huang, Y.; Wang, M.; Yu, M.; Zhu, Y.; Wu, J. PVD amorphous carbon coated 3D NiCo₂O₄ on carbon cloth as flexible electrode for both sodium and lithium storage. *Carbon* **2017**, *125*, 375–383. [[CrossRef](#)]
25. Wang, X.; Zhang, M.; Liu, E.; He, F.; Shi, C.; He, C.; Li, J.; Zhao, N. Three-dimensional core-shell Fe₂O₃@carbon/carbon cloth as binder-free anode for the high-performance lithium-ion batteries. *Appl. Surf. Sci.* **2016**, *390*, 350–356. [[CrossRef](#)]
26. Young, C.; Wang, J.; Kim, J.; Sugahara, Y.; Henzie, J.; Yamauchi, Y. Controlled Chemical Vapor Deposition for Synthesis of Nanowire Arrays of Metal-Organic Frameworks and Their Thermal Conversion to Carbon/Metal Oxide Hybrid Materials. *Chem. Mater.* **2018**, *30*, 3379–3386. [[CrossRef](#)]
27. Gu, X.; Chen, L.; Liu, S.; Xu, H.; Yang, J.; Qian, Y. Hierarchical core-shell α -Fe₂O₃@C nanotubes as a high-rate and long-life anode for advanced lithium ion batteries. *J. Mater. Chem. A* **2014**, *2*, 3439–3444. [[CrossRef](#)]
28. Gao, G.; Wu, H.; Ding, S.; Lou, X. Preparation of carbon-coated NiCo₂O₄@SnO₂ hetero-nanostructures and their reversible lithium storage properties. *Small* **2015**, *11*, 432–436. [[CrossRef](#)]
29. Grote, F.; Zhao, H.; Lei, Y. Self-supported carbon coated TiN nanotube arrays: Innovative carbon coating leads to an improved cycling ability for supercapacitor applications. *J. Mater. Chem. A* **2015**, *3*, 3465–3470. [[CrossRef](#)]
30. Mo, Y.; Ru, Q.; Song, X.; Guo, L.; Chen, J.; Hou, X.; Hu, S. The sucrose-assisted NiCo₂O₄@C composites with enhanced lithium-storage properties. *Carbon* **2016**, *109*, 616–623. [[CrossRef](#)]
31. Zhao, W.; Qi, Y.; Dong, J.; Xu, J.; Wu, P.; Zhang, C. New insights into the structure-property relation in ZnCo₂O₄ nanowire and nanosheet arrays. *J. Alloy Compd.* **2020**, *817*, 152692. [[CrossRef](#)]
32. Feng, J.; Li, Q.; Wang, H.; Zhang, M.; Yang, X.; Yuan, R.; Chai, Y. Hexagonal prism structured MnSe stabilized by nitrogen-doped carbon for high performance lithium ion batteries. *J. Alloy Compd.* **2019**, *789*, 451–459. [[CrossRef](#)]
33. Qi, Y.; Du, N.; Zhang, H.; Wu, P.; Yang, D. Synthesis of Co₂SnO₄@C core-shell nanostructures with reversible lithium storage. *J. Power Sources* **2011**, *196*, 10234–10239. [[CrossRef](#)]
34. Jiang, T.; Tian, X.; Gu, H.; Zhu, H.; Zhou, Y. Zn₂SnO₄@C core-shell nanorods with enhanced anodic performance for lithium-ion batteries. *J. Alloy Compd.* **2015**, *639*, 239–243. [[CrossRef](#)]
35. Yan, Z.; Sun, Z.; Yue, K.; Li, A.; Qian, L. CoO/ZnO nanoclusters immobilized on N-doped 3D reduced graphene oxide for enhancing lithium storage capacity. *J. Alloy Compd.* **2020**, *836*, 155443. [[CrossRef](#)]
36. Zhang, L.; Zhu, S.; Li, X.; Fang, H.; Wang, L.; Song, Y.; Jia, X. 3D porous ZnCo₂O₄@NiO on nickel foam as advanced electrodes for lithium storage. *Ionics* **2019**, *26*, 2157–2164. [[CrossRef](#)]
37. Bai, J.; Li, X.; Liu, G.; Qian, Y.; Xiong, S. Unusual Formation of ZnCo₂O₄ 3D Hierarchical Twin Microspheres as a High-Rate and Ultralong-Life Lithium-Ion Battery Anode Material. *Adv. Funct. Mater.* **2014**, *24*, 3012–3020. [[CrossRef](#)]
38. Zhu, Y.; Cao, C.; Zhang, J.; Xu, X. Two-dimensional ultrathin ZnCo₂O₄ nanosheets: General formation and lithium storage application. *J. Mater. Chem. A* **2015**, *3*, 9556–9564. [[CrossRef](#)]
39. Gao, S.; Yang, L.; Liu, Z.; Shao, J.; Qu, Q.; Hossain, M.; Wu, Y.; Adelhelm, P.; Holze, R. Carbon-Coated SnS Nanosheets Supported on Porous Microspheres as Negative Electrode Material for Sodium-Ion Batteries. *Energy Technol.* **2020**, *8*, 2000258. [[CrossRef](#)]
40. Li, D.; Zhang, J.; Ahmed, S.M.; Suo, G.; Wang, W.A.; Feng, L.; Hou, X.; Yang, Y.; Ye, X.; Zhang, L. Amorphous carbon coated SnO₂ nanosheets on hard carbon hollow spheres to boost potassium storage with high surface capacitive contributions. *J. Colloid Interface Sci.* **2020**, *574*, 174–181. [[CrossRef](#)]
41. Li, F.; Zou, Q.; Xia, Y. CoO-loaded graphitizable carbon hollow spheres as anode materials for lithium-ion battery. *J. Power Sources* **2008**, *177*, 546–552. [[CrossRef](#)]

42. Zhang, L.; Hu, P.; Zhao, X.; Tian, R.; Zou, R.; Xia, D. Controllable synthesis of core-shell Co@CoO nanocomposites with a superior performance as an anode material for lithium-ion batteries. *J. Mater. Chem.* **2011**, *21*, 18279. [[CrossRef](#)]
43. Xiong, S.; Chen, J.S.; Lou, X.W.; Zeng, H.C. Mesoporous Co₃O₄ and CoO@C Topotactically Transformed from Chrysanthemum-like Co(CO₃)_{0.5}(OH)·0.11H₂O and Their Lithium-Storage Properties. *Adv. Funct. Mater.* **2012**, *22*, 861–871. [[CrossRef](#)]
44. Wang, Y.F.; Zhang, L.J. Simple synthesis of CoO-NiO-C anode materials for lithium-ion batteries and investigation on its electrochemical performance. *J. Power Sources* **2012**, *209*, 20–29. [[CrossRef](#)]
45. Shi, W.; Zhao, H.; Lu, B. Core-shell ZnCo₂O₄@TiO₂ nanowall arrays as anodes for lithium ion batteries. *Nanotechnology* **2017**, *28*, 165403. [[CrossRef](#)]
46. Wang, Y.; Zhu, X.; Liu, D.; Tang, H.; Luo, G.; Tu, K.; Xie, Z.; Lei, J.; Li, J.; Li, X.; et al. Synthesis of MOF-74-derived carbon/ZnCo₂O₄ nanoparticles@CNT-nest hybrid material and its application in lithium ion batteries. *J. Appl. Electrochem.* **2019**, *49*, 1103–1112. [[CrossRef](#)]
47. Giri, A.K.; Pal, P.; Ananthakumar, R.; Jayachandran, M.; Mahanty, S.; Panda, A.B. 3D Hierarchically Assembled Porous Wrinkled-Paper-like Structure of ZnCo₂O₄ and Co-ZnO@C as Anode Materials for Lithium-Ion Batteries. *Cryst. Growth Des.* **2014**, *14*, 3352–3359. [[CrossRef](#)]
48. Bai, J.; Zhao, B.; Wang, X.; Ma, H.; Li, K.; Fang, Z.; Li, H.; Dai, J.; Zhu, X.; Sun, Y. Yarn ball-like MoS₂ nanospheres coated by nitrogen-doped carbon for enhanced lithium and sodium storage performance. *J. Power Sources* **2020**, *465*, 228282. [[CrossRef](#)]
49. Ran, L.; Luo, B.; Gentle, I.R.; Lin, T.; Sun, Q.; Li, M.; Rana, M.M.; Wang, L.; Knibbe, R. Biomimetic Sn₄P₃ Anchored on Carbon Nanotubes as an Anode for High-Performance Sodium-Ion Batteries. *ACS Nano* **2020**, *14*, 8826–8837. [[CrossRef](#)]
50. Zhang, Y.; Xu, G.; Liu, X.; Wei, X.; Cao, J.; Yang, L. Scalable In Situ Reactive Assembly of Polypyrrole-Coated MnO₂ Nanowire and Carbon Nanotube Composite as Freestanding Cathodes for High Performance Aqueous Zn-Ion Batteries. *ChemElectroChem* **2020**, *7*, 2762–2770. [[CrossRef](#)]
51. Li, W.; Dolocan, A.; Oh, P.; Celio, H.; Park, S.; Cho, J.; Manthiram, A. Dynamic behaviour of interphases and its implication on high-energy-density cathode materials in lithium-ion batteries. *Nat. Commun.* **2017**, *8*, 14589. [[CrossRef](#)] [[PubMed](#)]

Publisher's Note: MDPI stays neutral with regard to jurisdictional claims in published maps and institutional affiliations.



© 2020 by the authors. Licensee MDPI, Basel, Switzerland. This article is an open access article distributed under the terms and conditions of the Creative Commons Attribution (CC BY) license (<http://creativecommons.org/licenses/by/4.0/>).